Nanostrand Formation of Block Copolymers at the Air/Water Interface

Iryna I. Perepichka, Antonella Badia, and C. Geraldine Bazuin*

Département de Chimie, Centre de Recherche sur les Matériaux Auto-Assemblés (CRMAA/CSACS), Université de Montréal, Montréal (QC), Canada H3C 3J7

ARTICLE

ABSTRACT Langmuir—Blodgett monolayers consisting of a network of nanostrands have occasionally been reported in the literature, but are often coexistent with other morphologies, which is not useful for potential applications. With the use of PS-P4VP/PDP, a polystyrene-poly(4-vinyl pyridine) diblock copolymer of 12 mol % VP content mixed with 3-pentadecylphenol, it is shown that the disordered nanostrand network morphology can be obtained reproducibly and uniformly over large surface areas by spreading chloroform solutions of relatively high copolymer concentration. Use of a more slowly evaporating spreading solvent, 1,1,2,2-tetrachloroethane, and a low subphase temperature, 8—9 °C, results in much more densely aligned nanostrands. Poorly spreading solvents such as nitrobenzene produce the well-known fingerprint pattern often observed in spin- or dip-coated thin films of block copolymers. A mechanism for nanostrand network formation is proposed that involves the momentary formation of a fingerprint morphology in spreading drops followed by its breakup at the level of the mobile P4VP/PDP stripes as spreading continues, leaving P4VP-anchored PS nanostrands floating on the water surface.

KEYWORDS: nanostrand network · nanostructured monolayers · Langmuir—Blodgett · air/water interface · block copolymers · PS-P4VP · PDP

Nanotechnology relies on the ability to construct very precise nanostructures or nano-objects with well-defined shapes, sizes, and long-range order.[1,2] One of the most important methods to achieve this is the self-assembly of suitably designed molecules. This approach is privileged by nature to produce very complex but exquisitely designed biological structures. For materials scientists, block copolymers are a material of choice for achieving nanostructures based on phase separation between dissimilar blocks.[3−6] The size, shape, and order of the nanostructures can be tuned by changing the absolute and relative block lengths, by adding other substances that selectively associate with or modify the nature of one of the blocks, or by manipulating preparation conditions.[3−6]

Many nanotechnological applications of nanostructured polymers—ranging from nanoporous membranes to components in active nanodevices—require the polymer to be in the form of thin films with well-ordered nanopatterns.[6] One way to obtain solid-supported (ultra)thin nanopatterned films is by the Langmuir−Blodgett (LB) technique. This involves spreading a polymer solution at the air/water interface in a Langmuir trough, laterally compressing the available surface in a controlled manner with movable barriers, and transferring the monolayer film to a solid substrate. A common pattern obtained in this way, generally from amphiphilic diblock copolymers with relatively large hydrophilic block sizes, is composed of nanodots (also called spherical surface micelles) that tend to have two-dimensional hexagonal order.[7−14] The elevated core of these nanodots is formed from the condensed hydrophobic block that avoids the aqueous surface; it is surrounded laterally (and underneath) by the hydrophilic block that is spread as a monolayer on the water surface. When the hydrophilic block is much smaller than the hydrophobic block, elongated or cylindrical-type nanostructures (also termed spaghetti, ribbons, rods, worms, strands, stripes, wires) with various length-to-width aspect ratios can be obtained. Here, the elevated hydrophobic block in elongated form is surrounded on both sides (and underneath) by the flat hydrophilic block, as shown in Figure 1.[8−12] For still smaller hydrophilic blocks, variably sized planar aggregates (also termed pancakes, continents, islands), where the hydrophilic block resides mainly between the hydrophobic block and the water surface, usually form.[8−12] In contrast to the nanodot aggregates, which are relatively uniform in size, the latter two types of aggregates not only tend to have extensive size variability but also frequently occur together and/or mixed with nanodots

*Address correspondence to geraldine.bazuin@umontreal.ca.

Received for review June 11, 2010 and accepted October 18, 2010.

Published online October 27, 2010.
10.1021/nn101318e

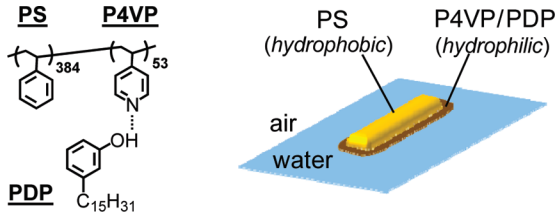

Figure 1. Molecular structure of PS-P4VP/PDP (left) and schematic representation of a segment of an elongated aggregate at the air/water interface (right).

and/or other nanoforms such as rings and chains.[8−11,15−18] Besides block composition and block ratio variation (which can include the addition of block-selective substances), strategies based on preparative conditions can be used to generate various nanostructures in LB films; for example, "nano-donuts" were formed by spreading a vesicular solution of an amphiphilic triblock copolymer onto a high pH subphase.[19]

Among the elongated nanostructures, those with very high aspect ratios have particular interest. They have potential use, for example, for forming long nanowires by templating the deposition of metals[20−22] or, as an alternative to electrospinning techniques, for producing nanofibers for various applications including medical.[23] A network or mesh of nanostrands (dubbed "nanostrand network morphology"[24]) composed of interconnected strands with relatively few ends, may be envisaged for, for example, constructing novel nanoseparation membranes by multilayer LB transfers of monolayers with this pattern. However, these nanostructures can be useful only if they are highly reproducible and "pure".

In this paper, we focus on the optimization of experimental conditions that favor reproducible patterns of long nanostrands or nanostrand networks with high surface coverage. This pattern and, more generally, related patterns containing high aspect ratio strands obtained at the air/water interface have been reported in the literature much less frequently than have surface micelles or nanodots. They have been observed in diblock copolymers including blends,[10,11,15−18,24−28] as well as in triblock[29,30] and starblock[31−33] polymers. In part, this relative infrequency is in line with the fact that strand- or rodlike patterns of any kind occur over a relatively narrow range of block copolymer composition.[9−12] When it is reported, it is often mixed with one or more additional morphologies, whether intimately or in the form of partial surface coverage.

We previously reported that the nanostrand network pattern can be obtained with high surface coverage using a polystyrene-*b*-poly(4-vinyl pyridine) (PS-P4VP) block copolymer (12 mol % VP content) mixed with 3-*n*-pentadecylphenol (PDP),[24] which hydrogen bonds to the VP block to form a "supramolecular complex"[34] (Figure 1). This pattern was obtained under conditions dubbed the "solvent-assisted procedure" where the PS-P4VP/PDP solution was spread very rapidly on the water surface, followed immediately by surface compression (typically to 10 mN/m) without waiting for the spreading solvent to evaporate. If the barriers were compressed after waiting for complete solvent evaporation or if the LB monolayer transfer took place at low surface pressure (typically less than 5 mN/m), a morphology composed primarily of nanodots mixed with planar aggregates was obtained. That the "solvent-assisted procedure" worked to produce the nanostrand network pattern was attributed to sufficient mobility maintained in the system, due to the presence of spreading solvent, and that it could respond to changing surface pressure conditions and adopt the nanostrand network morphology that appeared to be the preferred morphology at higher surface pressure. This is in accord with the similar explanation given by Seo *et al.*[25] for a blend of polystyrene-*b*-poly(ferrocenylsilane) (PS-PFS) and polystyrene-*b*-poly(2-vinyl pyridine) (PS-P2VP) (4:1 FS:VP molar ratio), which also showed a transition from predominantly spherical to nanostrand network morphology on increasing the surface pressure. Mobility allowing the change in morphology in this case was attributed to the plasticizing action of the low-T_g majority component PS-PFS.

A disadvantage of the "solvent-assisted procedure" is its reliance on rapid action that is prone to be user-dependent and thus susceptible to irreproducibility. Therefore, it is desirable to seek alternative conditions that allow the target morphology to be obtained using easily controlled standard procedures. This paper describes experimental conditions that optimize the nanostrand morphology at the air/water interface, using the same PS-P4VP/PDP system as for the solvent-assisted procedure (12 mol % VP, equimolar or near-equimolar VP:PDP molar ratio).[24] The main variables investigated are solution concentration, choice of spreading solvent, and subphase temperature. We will show not only that the nanostrand network can be obtained almost exclusively over very large surface areas but also that nanostrands with very little branching and high mutual alignment are achievable. Furthermore, the observation of a fingerprint morphology when using poorly spreading solvents suggests a novel mechanism for the formation of the nanostrand network.

RESULTS AND DISCUSSION

Copolymer Solution Concentration Using Chloroform as the Spreading Solvent. One obvious change that occurs during barrier compression in the solvent-assisted technique used previously by us[24] is an effective increase in the surface concentration (density) of the polymer. This led us to investigate, first of all, the effect of the concentration of the spread copolymer solution on the morphology of the monolayer films when using the standard Langmuir technique that includes waiting for complete solvent evaporation before barrier compression.

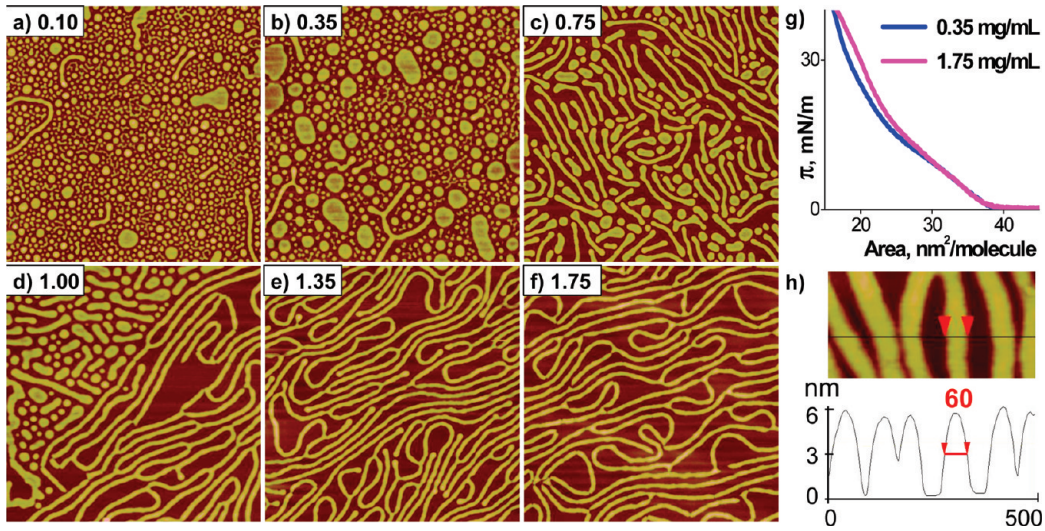

Figure 2. (a−f) AFM height images (3 × 3 μm²) of LB monolayers of PS-P4VP/PDP (1.0:1.0) formed at 20 °C from chloroform solutions of the copolymer concentrations (in mg/mL) indicated, and transferred to mica at π = 10 mN/m. (g) Langmuir compression isotherms of PS-P4VP/PDP. (h) Cross-section of height image (250 × 500 nm²).

Figure 2a−f presents AFM images of monolayer films of PS-P4VP/PDP (1.0:1.0 VP:PDP molar ratio) prepared from chloroform solutions having copolymer concentrations that range from 0.10 to 1.75 mg/mL for identical total mass of material spread, and transferred to mica at a surface pressure (π) of 10 mN/m. These images show that nanodots and planar aggregates (up to 500 nm in diameter) are predominant at lower concentrations (0.10 and 0.35 mg/mL), in agreement with what we found previously for the 0.35 mg/mL solution using the standard Langmuir procedure (the same concentration that produced the nanostrand network using the "solvent-assisted procedure").[24] At intermediate concentrations (0.75 and 1.00 mg/mL), elongated or rodlike structures (along with some nanostrand network for the higher concentration) appear, but they tend to be short and are mixed with nanodots and other small (irregular) aggregates. At the highest concentrations (1.35 and 1.75 mg/mL), the nanostrand network, composed of strands [6 ± 1 nm in height, 60 ± 10 nm in width at half-height (Figure 2h), and up to more than 10 μm in length] that are more or less laterally disordered and interconnected by three-branch junction points, is the almost exclusive morphology observed. Dangling strand ends are also visible, especially for the lower concentration solution. The same copolymer without PDP does not lead to nanostrand formation, but to variably sized rounded aggregates at low spreading solution concentration and to very large platelets at high concentration. It is noteworthy that the Langmuir isotherms (Figure 2g), discussed previously in comparison with those for PS-P4VP and PDP,[24] are very similar for low and high concentrations, especially at the pressures of 5 and 10 mN/m typically employed for film transfer. This indicates that the morphological differences in the films do not significantly impact the surface pressure evolution with molecular area for the concentration range investigated.

Clearly, use of a sufficiently high spreading solution concentration is a key parameter for obtaining the nanostrand network morphology. The importance of concentration is illustrated also by another experiment involving a modified Langmuir−Schaefer (LS) technique,[15] where a single drop (*ca.* 10 μL) of a PS-P4VP/PDP (1.0:1.3) solution of high concentration (2.05 mg/mL) was deposited on the water surface above one end of a submerged substrate. After removal of the water, AFM images, shown in Figure 3, were taken at defined distances from the spot above which the drop was deposited. This series of images shows optimal nanostrand network formation within a few centimeters of the deposition spot and short nanostrands mixed with nanodots, along with poor surface coverage, in the areas furthest from the deposition spot. This morphology evolution can be correlated with a decrease in local polymer concentration (density) in moving away from the deposition spot. The LS film morphology also shows that the nanostrands are not induced by the LB (vertical) transfer. Given that this LS experiment (and some others described below) was conducted with solutions having a small excess of PDP relative to VP, it must be specified that LB experiments at various VP:PDP molar ratios, to be described in detail in a subsequent paper, show that there is no difference in morphology obtained for 1.0:1.0 to 1.0:1.3 molar ratios.

The influence of the concentration of the spreading solution on the LB film morphology was observed previously by Devereaux and Baker[15] and by Cheyne and Moffitt[16,17] for PS-PEO [PEO: poly(ethylene oxide)] diblock copolymers. In the first case,[15] where PEO constitutes 7 wt % of the polymer, low concentration favors nanodot formation and high concentration favors planar aggregates ("continents"), although both morphol-

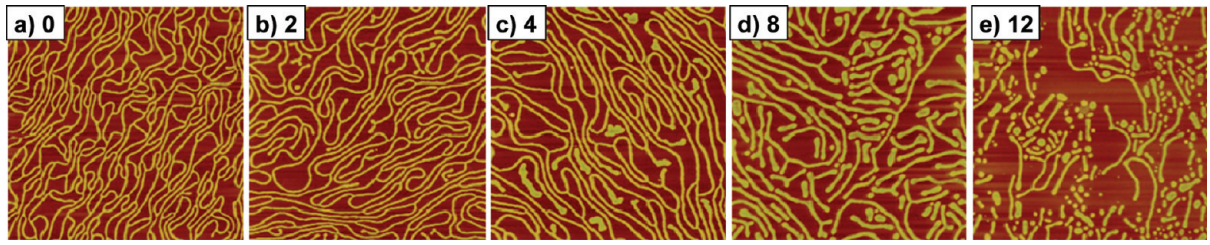

Figure 3. AFM images (5 × 5 μm²) of a Langmuir−Schaefer film of PS-P4VP/PDP (1.0:1.3) obtained from a single drop of $CHCl_3$ copolymer solution having a concentration of 2.05 mg/mL. The numbers indicate the position in centimeters of the area imaged relative to the area where the drop was deposited.

ogies are generally coexistent. Nanostrands ("spaghetti") are also present for most concentrations, but cover less than half, often only a small fraction, of the film area. In the second case,[16,17] involving 11.4 wt % PEO, mixed morphologies of nanodots and nanostrands were observed at most concentrations studied, along with a high proportion of rings and chains at the lowest concentration and a network of what were interpreted as dewetted rims at the highest concentration.

Other Spreading Solvents. Chloroform is the most common spreading solvent used to prepare Langmuir monolayers. However, solvent can be used as a tool to maintain mobility in the system for longer times by turning to ones that evaporate more slowly. To this end, we investigated the use of 1,2-dichloroethane ($C_2H_4Cl_2$) and 1,1,2,2-tetrachloroethane ($C_2H_2Cl_4$), chemically similar to chloroform but with lower vapor pressures (vp = 160, 87, and 8 mmHg at 20 °C for $CHCl_3$, $C_2H_4Cl_2$, and $C_2H_2Cl_4$, respectively), as well as hexachloropropene (C_3Cl_6; vp = 4 mmHg at 100 °C) and nitrobenzene ($PhNO_2$; vp = 0.15 mmHg at 20 °C). It was noted that $C_2H_2Cl_4$ solution appears to spread more slowly than $CHCl_3$ and $C_2H_4Cl_2$ solutions; that is, the spreading $C_2H_2Cl_4$ drops were visible by eye for a few seconds, in contrast to drops of the other two solvents. $PhNO_2$ spreads relatively little (and is malodorous), whereas C_3Cl_6 does not spread at all and was therefore mixed with $C_2H_2Cl_4$ (50/50 v/v), which allowed limited spreading. Langmuir isotherms using these solvents, given in the Supporting Information, are all similar in form to that using $CHCl_3$, with the shift to somewhat lower molecular areas for $C_3Cl_6/C_2H_2Cl_4$ probably a consequence of its very incomplete spreading. Overall, these isotherms again indicate relatively little sensitivity to the morphological differences described below.

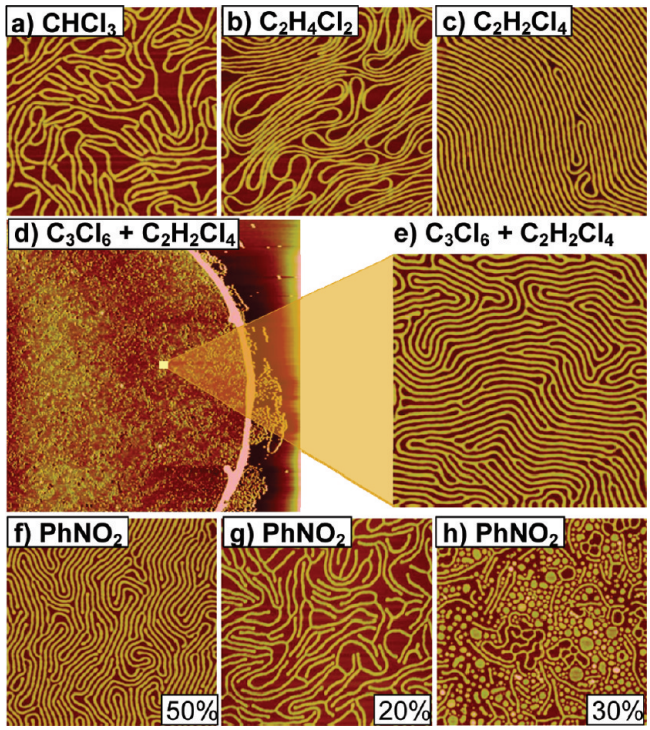

Figure 4. AFM height images of PS-P4VP/PDP (1.0:1.2) monolayers deposited from 1.80−1.90 mg/mL solutions for the spreading solvents indicated (T = 20−21 °C, π = 5 mN/m). Scan size: (a−c,e−h) 3 × 3 μm²; (d) 100 × 100 μm². Numbers refer to % area covered by the morphology shown (>80% if not otherwise indicated).

AFM images of PS-P4VP/PDP (1.0:1.2) LB films obtained at low surface pressure (5 mN/m) using the different spreading solvents with high copolymer concentration (1.80−1.90 mg/mL) are compared in Figure 4. The nanostrand morphology is obtained from both $C_2H_4Cl_2$ and $C_2H_2Cl_4$ solutions, but with differing density and alignment of the strands. The morphology obtained using $C_2H_4Cl_2$ is similar to that using $CHCl_3$, with the nanostrands in significant lateral disorder in both cases, with only a mildly greater degree of strand alignment and density for $C_2H_4Cl_2$. In addition, almost no interjection of other morphological features was observed for $C_2H_4Cl_2$ (based on two trials) compared with 5 to 20% for $CHCl_3$ (considering many different trials). In contrast, when using $C_2H_2Cl_4$, which has a much lower vapor pressure than the other two solvents and thus evaporates significantly more slowly from the water surface, strand density is generally close to maximal due to a very high degree of nanostrand alignment along with few branching points and strand ends. This results in smooth and uniform strands, composed of elevated PS stripes (light regions in the AFM phase image) separated by monolayer-thin P4VP/PDP stripes (dark regions in the phase image), that are extremely long, more than 30 μm. There are also spaces (often large) with no material on the mica substrate, indicating incomplete spreading, as well as a few places with more disordered strands. It may be added that no correlation

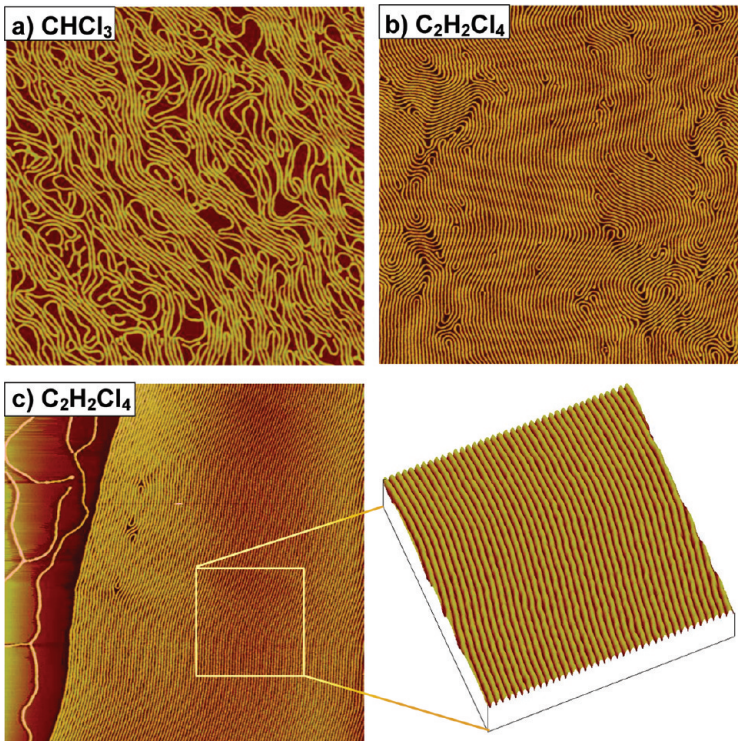

Figure 5. AFM height images of PS-P4VP/PDP (1.0:1.3) monolayers spread at 8 °C, using the solvents indicated and a copolymer solution concentration of 1.85 mg/mL, and transferred to mica at $\pi = 5$ mN/m. Scan size: (a,b) 8 × 8 μm²; (c) 10 × 10 μm² (zoom: 3 × 3 μm²).

was found between strand alignment and substrate withdrawal direction.

The reduced spreading ability of $PhNO_2$ and especially $C_3Cl_6/C_2H_2Cl_4$ results in large circumscribed areas of material (visible by optical microscopy and also observed using the LS technique), as illustrated in Figure 4d. Within these areas, a dense form of the nanostrand network, composed of highly mutually aligned nanostrands, is observed (Figure 4e,f). This pattern actually resembles the "fingerprint" texture often observed in thin block copolymer films obtained by spin- and dip-coating, including in films of similar thickness to LB monolayers.[21,22,35−41] For $C_3Cl_6/C_2H_2Cl_4$, there is little interjection of other morphologies, whereas for $PhNO_2$ (Figure 4f−h), the dense fingerprint texture (*ca.* 50%) is the main texture observed, but there are also areas of the more disordered nanostrand network (*ca.* 20%) and areas of a mixed morphology (*ca.* 30%) of nanodots/short nanostrands/planar aggregates (when large, the latter sometimes contain holes as in "nanofoams"[42] and occasionally appear in the form of interconnected "dewetted rims"[17]).

Subphase Temperature. Reducing the temperature of the subphase, which reduces the evaporation rate of the spreading solvent, is another way to prolong the presence of solvent and therefore the time period of polymer mobility. The effect of a low subphase temperature on the morphology using $C_2H_2Cl_4$ as the spreading solvent is shown in Figure 5b,c. In comparison with the morphology obtained at 20−21 °C, that obtained at 8−9 °C shows highly mutually aligned strands with far fewer loops and turns. Furthermore, the densely aligned nanostrand pattern extends over areas that are much larger, as shown in Figure 5b for an 8 × 8 μm² region and in the Supporting Information for a 30 × 30 μm² region (Figure SI-2). No areas with the disordered nanostrand network morphology were observed, but there were more and larger empty areas, in line with the greater packing density of the areas with material. In contrast, when using $CHCl_3$, lowering the temperature to 8−9 °C has only a minor effect on the morphology (Figure 5a): here, the nanostrands, while also extending over large areas, remain disordered on the 2D surface, with many loops, turns, branching points and loose packing, and essentially only the number of strand ends is reduced. Use of a dilute (0.37 mg/mL) $C_2H_2Cl_4$ solution does not yield the dense nanostrand pattern, either at ambient or low temperature (instead, short nanostrands mixed with nanodots and planar aggregates are observed, as shown in the Supporting Information, Figure SI-3), indicating again the key role of spreading solution concentration.

The 10 × 10 μm² image shown in Figure 5c, where the edge of a densely aligned nanostrand domain was captured, is also of interest. First, it shows that the aligned strands are highly parallel to the domain edge, which suggests that the nanostrand pattern is susceptible to macroscopic alignment. Indeed, it has recently been shown that macroscopic alignment is achievable on chemically patterned substrates,[43] although this was for LB transfer of the already-formed nanostrand network, whereas the alignment shown in Figure 5c presumably occurred in the course of morphology formation on the water surface. Second, only three defects, two single-loop ones and one double-loop one (which can also be considered as two neighboring defects, since each isolated single-loop defect is in the same strand as one loop in the paired defect), are visible in the area shown. Third, there are a few isolated nanostrands in the area outside of the dense nanostrand domain, which will be commented on in the discussion that follows.

The widths and heights of the nanostrands obtained using the different solvents and at the two different temperatures appear relatively constant within experimental uncertainty. Considering various

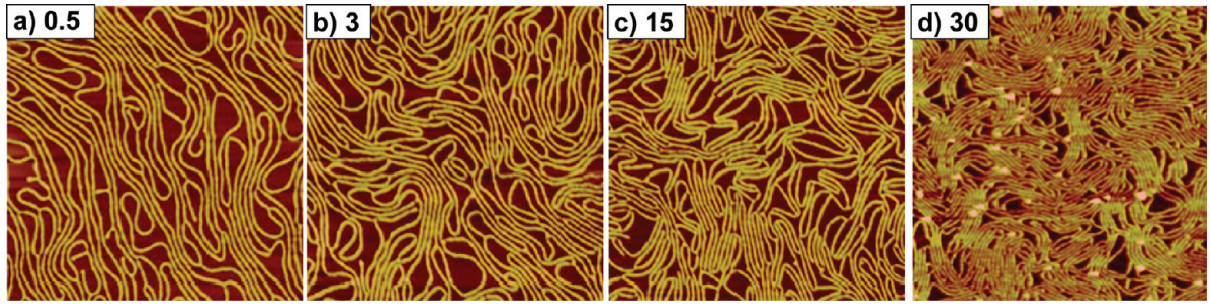

Figure 6. AFM height images (5 × 5 μm²) of PS-P4VP/PDP (1.0:1.0) monolayers spread from a 1.80 mg/mL $CHCl_3$ solution (subphase temperature, 20 °C) and transferred to mica at the surface pressures (in mN/m) indicated.

measurements of sufficiently isolated strand segments, heights are generally 6 ± 1 nm and the widths at half-height 70 ± 20 nm (where the higher numbers are most likely due to imaging with blunter AFM tips). These dimensions are comparable to those found for other PS-based block copolymers showing cylindrical-type morphology in LB films,[8,9,15,16] with the height being similar to the (collapsed) random coil radius of the PS block segment as in ref 8 and reflecting the hydrophobicity of PS, and the width more than ten times larger, reflecting laterally stretched PS chains[8] and/or the overlapping of several PS chains[16] across the strand. Periodicities of parallel, closely spaced strand segments are generally in the 70−100 nm range (78 nm for the zoomed image in Figure 5c, where the large number of parallel strands allows a particularly accurate measurement). This corresponds to closest approach spacings between the strands of roughly 30 nm, similar to twice the extended length of the P4VP block segment (13 nm). This is consistent with P4VP being located as a surface-adsorbed monolayer alongside the strands (and therefore too thin to distinguish from the bare surface in AFM images of isolated strand segments), again in accordance with previous studies, particularly on a system based on *n*-alkylated PS-P4VP block polyelectrolytes where the alkyl chains are covalently bonded to the P4VP block, therefore with a molecular architecture like that of the present PS-P4VP/PDP system (albeit ionic).[8,9] Presumably, PDP hydrogen-bonded to P4VP lies more or less parallel to the water surface at low pressures, as determined by X-ray and neutron reflectivity for the alkyl chains of *n*-alkylated PS-P4VP (with nanodot morphology).[44,45]

Surface Pressure. All of the LB films imaged above were transferred at relatively low surface pressure (≤10 mN/m). It is of interest to examine possible effects of this parameter on the film morphology, shown in Figures 6 and 7 for spreading solvents, $CHCl_3$ and $C_2H_2Cl_4$, respectively. First, it must be emphasized that low concentration solutions (0.35 mg/mL) do not yield the nanostrand network morphology even at high transfer surface pressure, in accordance with what we reported previously.[24] On the other hand, as shown in Figure 6, spreading from a high concentration solution (1.75−1.80 mg/mL) gives nanostrands from very low (0.5 mN/m) up to high (at least 40 mN/m) surface pressure. Only strand density tends to increase with surface pressure (most obvious when comparing very different surface pressures), with separated strand widths and heights unaffected. This indicates that the nanostrand network forms soon after solution deposition and that barrier compression simply pushes the network strands closer together. At 30−40 mN/m, the transferred film appears buckled in some places, especially where the nanostrands make sharp turns (observed as bright spots in the AFM height images, indicating greater heights; see Figures 6d and 7b−d). These buckled films remain buckled after barrier expansion to low surface pressure and open cracks appear within the dense nanostructured areas throughout the film, illustrated by the image in Figure 7d, indicating significant irreversible interstrand "sticking".

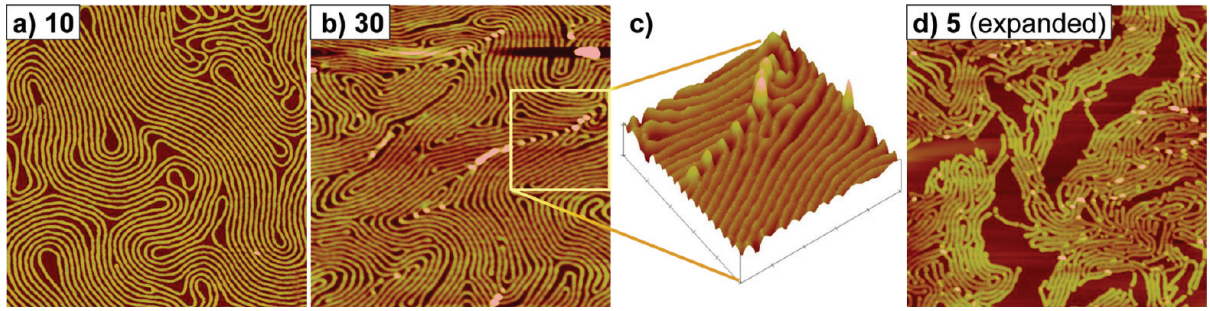

Figure 7. AFM height images (a,d, 5 × 5 μm²; b, 3 × 3 μm²; c, 1 × 1 μm²) of PS-P4VP/PDP (1.0:1.3) monolayers spread from a 1.90 mg/mL $C_2H_2Cl_4$ solution (subphase temperature, 9 °C), and transferred to mica at the surface pressures (in mN/m) indicated: (a−c) in compression cycle, (d) after expansion from 30 mN/m.

General Discussion and Proposed Mechanism of Nanostrand Network Formation. The above results show that it is possible, under suitable conditions, to obtain the nanostrand morphology from PS-P4VP/PDP block copolymers over large surface areas quite uniformly and reproducibly. One of these conditions, not investigated here, is the proper choice of block ratio that favors elongated nanostructures (12 mol % P4VP/PDP content worked very well in the present case), just as was found for other systems investigated as a function of block copolymer composition.[8−12] In particular, LB monolayers of architecturally similar *n*-decylated PS-P4VP show cylindrical-like morphology (*i.e.*, relatively short nanostrands) in the 6−14 mol % VP range.[9] (The morphology evolution in LB films of PS-P4VP with change in block ratio both with and without PDP present, showing the restricted composition range in which nanostrand morphology is found, will be addressed in a forthcoming paper.) The nanostrand morphology is thus considered to be a special case of the general class of elongated morphologies observed in LB block copolymer monolayers (see Introduction), where the illustration in Figure 1 represents a nanostrand segment; that is, an elevated PS core forms the backbone of the nanostrands and this backbone is lined alongside (and probably underneath) by a P4VP/PDP monolayer adsorbed to the water surface.

The present work has shown, using the standard Langmuir technique, that the concentration of the spreading solution is a key parameter for obtaining the nanostrand morphology with PS-P4VP/PDP (12 mol %) (discussed further below). In addition, use of a less volatile spreading solvent and lowering of the subphase temperature are favorable to nanostrand formation as well as to high mutual alignment of the strands. The latter can be attributed, at least in part, to the increased residence time of the spreading solvent on the water surface, which increases the period of polymer mobility during which self-assembly and morphology development can take place. Furthermore, the presence of PDP plays a role, since without it nanostrands are not found. First, it no doubt contributes to the total volume of the hydrophilic block and thus to the appropriate block composition favoring this morphology. In addition, its low molecular weight, amphiphilic, and liquid crystal character may be important for the high surface coverage of the nanostrand morphology. As a small molecule that is presumably largely hydrogen-bonded to VP as an effective side chain throughout the process, it can behave as an internal plasticizer for P4VP and thus contribute to mobility in the system (recognizing, however, that the hydrophilic P4VP itself maintains significant mobility on the water surface). As a liquid crystal when H-bonded to P4VP[34] and/or as an amphiphilic surfactant, it may also directly aid in the surface organization. An analogous effect was reported for the addition of a polar liquid crystal, 4′-pentyl-4-cyanobiphenyl, to a solution of an approximately symmetric PS-P4VP diblock copolymer, which was shown to facilitate the development of a highly regular nanodot array in LB films.[46]

In considering the complex monolayer-forming process during which the surface conditions continuously evolve, it must be kept in mind that the solution concentrations used are an order of magnitude smaller than the critical overlap concentration (greater than 50 mg/mL), as analyzed in ref 15 for a similar PS block molecular weight (7700 g/mol higher than in the present case), indicating the absence of entanglements initially. Then, as the drops spread and as solvent evaporates, the block copolymer chains tend to aggregate and possibly entangle at the level of the hydrophobic PS blocks, while undergoing morphological reorganization in response to their changing local concentration, to their increasing exposure to water and air, and to their increasingly ultrathin film confinement, until they are vitrified (partially or completely, or in distinct stages) or until final equilibrium is reached, whichever comes first.[47] Possibly, during a certain initial period of the solvent spreading/evaporation process, the system is in equilibrium with the instantaneous thermodynamic conditions until at some point it begins to lag behind, then increasingly so until parts or all of the system become frozen in. Only systems that maintain sufficient mobility throughout the entire process are at equilibrium with the final conditions of complete surface coverage, which is undoubtedly rare for polymers.

Baker and coll. and Moffitt and coll. have discussed previously how various morphologies including nanostrands are kinetic structures trapped by vitrification at different stages in the complex process.[15−17] This was supported by numerical simulations that showed that a sufficiently concentrated solution can go through a stage of (short) strandlike structures during drop spreading that, if vitrified before further evolution, compose the final morphology of the Langmuir film, but, if still mobile, break up into dots.[47] Applied to the present case, this picture indicates that drops of more concentrated PS-P4VP/PDP solution, implying initially high polymer density at the water surface, are more likely to achieve the strand morphology and, because less solvent is present, can become vitrified in this form before breakup into nanodots can occur. In contrast, many drops of more dilute solution (for the same total mass on the surface), implying lower polymer density at the water surface from the start, may not even go through the nanostrand stage,[47] or, if they do, there is enough solvent left to allow breakup into nanodots before vitrification sets in. Moffitt and coll. proposed another mechanism where the various morphologies in LB films are a consequence of dewetting phenomena that occur during the continuously evolving process following drop deposition, and that nanostrands, in particular, are formed from the breakup of dewetted rim networks

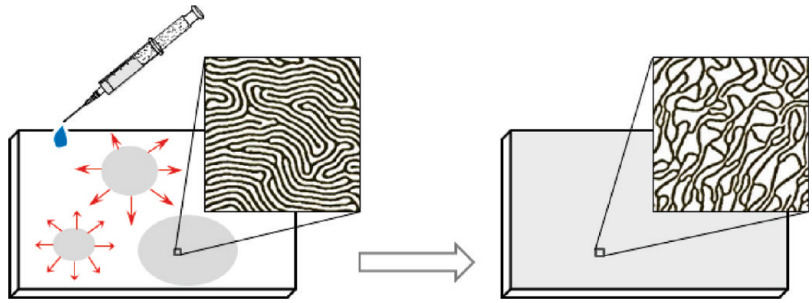

Figure 8. Model illustrating fingerprint to nanostrand network formation: the fingerprint morphology (left, with black and white stripes representing phase-separated PS and P4VP/PDP domains, respectively) forms in concentrated drops of PS-P4VP/PDP solution spreading on the water surface, with immobilization occurring in the hydrophobic PS stripes, then upon further spreading this fingerprint pattern disassembles at the level of the hydrophilic and mobile P4VP/PDP stripes to form the nanostrand network (right, with black lines representing floating, interconnected P4VP/PDP-lined PS nanostrands).

at their junction points.[17] On the other hand, Chang and coll. suggested that isolated surface micelles can be induced under special conditions (in their case by reducing the subphase pH, which ionizes the P2VP block) to aggregate into a necklace-type network[48] that may further coalesce[27] into a nanostrand network if sufficient mobility remains. This latter mechanism might perhaps apply to the morphology transition from nanodots to nanostrand network with increase in surface pressure that was observed for the PS-PFS/PS-P2VP blend reported in ref 25 (see Introduction).

The observation, in the present work, of the fingerprint morphology using poorly spreading solvents ($PhNO_2$ and $C_3Cl_6/C_2H_2Cl_4$) suggests still another possible mechanism of nanostrand formation. First, to comment on the fingerprint morphology itself, it should be pointed out that in poorly spreading solvents, the polymer density within the spreading drop remains high as the solvent evaporates and spreading is far from complete before immobility sets in. It is reasonable that, in these concentrated drops, the block copolymer can self-assemble into the same fingerprint morphology as observed under certain conditions for spin- or dip-coated films on hard polar surfaces (only partially understood for asymmetric diblock copolymers[21,39]). This fingerprint morphology (Figure 4d−f) is composed of meandering stripes of alternating PS and P4VP/PDP domains in a locally coherent film, probably also with a "wetting layer"[37] (a monolayer adsorbed to the polar substrate) of the hydrophilic block below the PS parts. (It should be noted that, because the film thickness is much smaller than the lateral periodicity, the fingerprint pattern can be viewed indifferently as a thin slice through either end-on stacked lamellae or horizontally lying cylinders of the phase-separated block copolymer.[8,35]) For $C_2H_2Cl_4$ as solvent, which spreads faster than $PhNO_2$ and $C_3Cl_6/C_2H_2Cl_4$ but not as fast as $CHCl_3$, and which has a relatively long residence time on the water surface compared to $CHCl_3$, the morphology obtained (Figure 4c) can be considered to be a more perfected version of the fingerprint morphology with fewer defects in the form of strand ends, forks and loops, allowing extensive mutual alignment of extremely long strands, especially at lower subphase temperature (Figure 5b,c) where the solvent resides for an even longer time. The greater spreading of $C_2H_2Cl_4$ compared to $PhNO_2$ and $C_3Cl_6/C_2H_2Cl_4$ may also allow more space for what can be considered as effective solvent annealing to take place, while still maintaining high polymer density during the self-assembly process.

What we now propose is the following mechanism for nanostrand formation, illustrated in Figure 8. First, spreading drops of sufficiently concentrated $CHCl_3$ solutions are considered to pass through a fingerprint morphology stage, the PS stripes become vitrified in this stage, then, as the drops continue to spread, the fingerprints break up (*i.e.*, disassemble) at the level of the hydrophilic P4VP/PDP stripes, which remain mobile (and unentangled, being relatively short) on the water surface. This allows the strands to separate from one another to float more or less individually on the water surface—within the constraints of the allowed space and of the interconnectivity at the level of the PS stripes (the latter leading to the network aspect)—as drop spreading continues until completion, thus forming the loosely structured (*i.e.*, disordered) nanostrand network morphology. The few such free strands observed in Figure 5c for $C_2H_2Cl_4$ at low subphase temperature can be interpreted as having separated in this way from the rest of the structure shown. This mechanism is analogous to what was obtained in bulk (3D) films of PS-P4VP/PDP having cylindrical PS domains in a P4VP/PDP matrix, where a selective solvent for PDP caused the disassembly of the cylindrical bulk structure into P4VP-coated nanofibers with PS cores (interestingly, with a PS core diameter of 25 nm, which compares well with the nanostrand widths taking into account the PS molecular weight, which is half that used in the present work).[49] Furthermore, the uniformity in width and height of the nanostrands is consistent with the characteristic lateral spacing of the fingerprint pattern. The interconnection of strands *via* triple-strand junctions and the random presence of dangling strands in the nanostrand network, as well as the great lengths and smooth

twists and turns of the nanostrands, are also consistent with what is observed in the fingerprint texture. Finally, the extensive coverage of the nanostrand network over the surface would reflect the uniformity of the fingerprint texture in essentially all of the spreading drops.

The fingerprint-to-nanostrand network mechanism is not necessarily to be construed as a replacement for the other mechanisms proposed in the literature. In other words, there may be more than one way to arrive at the nanostrand morphology: by direct polymer self-organization from a sufficiently concentrated and initially homogeneous solution spread on the air/water interface,[8,47] by the assembly of nanodots upon increasing the surface density of polymer when appropriate mobility is maintained in the system,[25,48] by the disassembly of a coherent film having a fingerprint morphology within spreading droplets of concentrated solution (this work), or from the breakup of a dewetted rim structure where the rims effectively concentrate the polymer material.[17] Future work should provide additional understanding of these different possibilities at the air/water interface.

CONCLUSIONS

Using the PS-P4VP/PDP block copolymer system with 12 mol % VP content, where the PDP small molecule hydrogen bonds to the P4VP block, we have shown that the disordered nanostrand network morphology with relatively few strand ends can be obtained reproducibly and uniformly over large surface areas using the standard Langmuir−Blodgett technique. A key condition for obtaining this morphology is the use of spreading solutions of relatively high polymer concentration, so that self-organization at the air/water interface takes place under conditions of high polymer density. The use of tetrachloroethane instead of chloroform as the spreading solvent and a low subphase temperature, both of which retard solvent evaporation and thus maintain polymer mobility at the water surface for longer periods, results in a pattern of densely packed, highly aligned nanostrands. This pattern may be considered as a perfected version of the nanostrand network due to solvent annealing. The poorly spreading solvents used, nitrobenzene and hexachloropropene/tetrachloroethane (50/50), produce the well-known fingerprint pattern observed in spin- and dip-coated thin films of block copolymers. The latter pattern leads to the proposal that a possible mechanism for nanostrand network formation, besides others proposed in the literature, is *via* the fingerprint morphology that may form in the course of the spreading of concentrated drops. The hydrophobic PS stripes become vitrified in this morphology, whereas the hydrophilic P4VP/PDP stripes remain mobile, such that, as drop spreading continues, the stripes disassemble at the level of these hydrophilic stripes, leaving P4VP-lined PS nanostrands free to float into the form of a disordered network on the water surface.

EXPERIMENTAL SECTION

Materials. Polystyrene-*b*-poly(4-vinyl pyridine) (PS-P4VP) with M_n(PS) = 40000 g/mol, M_n(PVP) = 5600 g/mol (384 S repeat units, 53 VP repeat units, 12 mol % VP content), and M_n/M_w = 1.09 was obtained from Polymer Source (Montreal, Canada), and used as received. 3-*n*-Pentadecylphenol (PDP) (Sigma-Aldrich, 90%) was recrystallized twice from hexane before use. Chloroform (HPLC grade, ≥99.8%; bp 61 °C), 1,2-dichloroethane (HPLC grade, 99.8%; bp 84 °C), nitrobenzene (ACS reagent grade, ≥99.0%; bp 210−211 °C), and hexachloropropene (96%; bp 209−210 °C), all obtained from Sigma-Aldrich, and 1,1,2,2-tetrachloroethane (GC, ≥98.0%; bp 144−146 °C) from Fluka, were used to prepare solutions for monolayer spreading. Ultrapure water (18.2 MΩ cm), used as the subphase in the Langmuir−Blodgett trough, was obtained by purification of distilled water with a Millipore Milli-Q Gradient system. Muscovite ruby mica (ASTM grade 2, B&M Mica, Flushing, NY, USA) was cleaved immediately before its immersion into the subphase.

Langmuir Isotherms and Monolayer Deposition. PS-P4VP and PDP, dissolved separately in the desired solvent, were mixed in the desired proportion (between 1.0:1.0 and 1.0:1.3 molar ratio VP:PDP), and left to stir overnight at room temperature in sealed volumetric flasks. It was noted that $C_2H_2Cl_4$ solutions, in contrast to the other solutions, were unstable over time, with more aged solutions giving very different morphologies compared to solutions that were freshly prepared up to a day old. Hydrogen-bonding of PDP to VP in $CDCl_3$ and $C_2D_2Cl_4$ solutions was confirmed by ^{1}H NMR spectroscopy, which shows that the sharp OH proton for pure PDP (located at 4.59 ppm in $CDCl_3$ and 4.65 ppm in $C_2D_2Cl_4$) undergoes extensive broadening with accompanying intensity decrease and a downfield shift (centered at *ca.* 5.15 and 4.80 ppm, respectively) in the presence of PS-P4VP, as shown in the Supporting Information (Figures SI-4 and SI-5).

A computer-controlled KSV 3000 Langmuir−Blodgett system with a platinum Wilhelmy plate sensing device (KSV Instruments, Helsinki, Finland) was used. The subphase temperature in the trough (150 × 518 mm) was maintained at 20−21 °C unless otherwise specified, using a refrigerated circulator (Isotemp 3016, Fisher Scientific). Solution was spread dropwise in a checkerboard pattern, using Hamilton microliter syringes: 50−200 μL for 0.35−2.05 mg/mL concentrations and 1 mL for 0.10 mg/mL concentration, where concentration is expressed in terms of block copolymer weight per volume of solvent. At least one drop was deposited within about 3−4 cm from the area above the submerged substrate(s). This was found to be important for the reproducibility of the observed film morphology for the more highly concentrated solutions for which as few as eight drops were necessary to reach the required total mass of material to spread on the water surface.

Following solvent evaporation (30−60 min for $CHCl_3$, 60−90 min for the other spreading solvents), surface pressure (π) *vs* mean molecular area (A) isotherms were obtained by symmetrical compression of the barriers at a speed of 10 mm/min (15 cm^2/min). All isotherms were run at least 2−3 times and showed good reproducibility.

Under the same conditions as for the isotherms and following a 20−30 min wait at the desired surface pressure (usually 5 or 10 mN/m) for barrier stabilization, LB films were deposited on mica substrates (sizes varying from 1 × 1.5 to 2.5 × 5 cm^2) that were vertically withdrawn from the subphase at a controlled speed (5 or 10 mm/min). The films were found to show good stability during the barrier stabilization step, with about a decrease in pressure of about 0.5 nm^2/molecule recorded. The transfer ratio was generally 1.0 ± 0.2. Other substrates besides mica [silicon wafer, quartz, and glass microscope slides, indium tin oxide (ITO) glass, gold, and highly ordered pyrolytic graphite (HOPG)]

were also tested and did not modify the basic morphology compared to that observed with mica (Supporting Information, Figure SI-6).

Occasionally, Langmuir−Schaefer (LS) films, where transfer was performed on a horizontally lying substrate, were also obtained. In another experiment, single-drop deposition[15] was combined with the LS technique. First, a mica substrate, whose length (*ca.* 14.5 cm) was close to the width of the trough, was placed on the trough floor, midway between and in parallel with the movable barriers. Then, the surface area was compressed to give zero surface pressure slightly below the onset of measurable pressure for the solution to be deposited as calculated from the π-A isotherm (159 cm^2, or 150 × 106 mm^2), and a single drop (*ca.* 10 μL) of 2.05 mg/mL PS-P4VP/PDP solution in $CHCl_3$ was deposited above one end of the substrate. After 60 min, the water was removed carefully by aspiration using the water pump.

AFM Imaging. The deposited films were dried in a clean box overnight at room temperature and then imaged in air by atomic force microscopy (AFM) in tapping mode using a multimode AFM with a Nanoscope IIIa controller (Digital Instruments/Veeco, Santa-Barbara, USA) and silicon probes (MikroMasch USA: rectangular, no aluminum coating on tip and backside, resonance frequency 265−400 kHz, tip curvature radius less than 10 nm; or Nanosensors: type PPP-NCH, nominal spring constant of 42 $N \cdot m^{-1}$, resonance frequency 330 kHz, tip radius of curvature <10 nm). Nanofeature dimensions were determined from height profiles across the strands. Widths were measured at half-height of sufficiently isolated strand segments. Heights were determined from the nanostrand summits relative to the flat areas between them. At least two separate experiments per condition were performed, and each LB film obtained was imaged (typically as 10 × 10 μm^2 images) at a minimum of 10 different places scattered over the film but avoiding the substrate edges. Generally, at least 90% of the images for a given experimental condition ("image set") show the same morphology. When a second (or, rarely, third) morphology is observed in 20% or more of the image set, this is stated in the text and, in some cases, illustrated. All transferred films are stable in air at ambient temperature (*i.e.*, no changes were observed in one-year old films compared to their freshly prepared state).

Acknowledgment. The financial support of NSERC Canada and FQRNT Québec is gratefully acknowledged. A.B. and I.I.P. acknowledge their membership in the FQRNT-supported Réseau québécois des matériaux de pointe (RQMP). I.I.P. thanks FQRNT for a Merit scholarship for foreign students and Université de Montréal for a final year scholarship. K. Borozenko is thanked for obtaining the isotherms in Supporting Information, Figure SI-1.

Supporting Information Available: Langmuir compression isotherms of PS-P4VP/PDP in different spreading solvents; AFM images of PS-P4VP/PDP monolayers spread from concentrated (enlarged area of Figure 5b) and dilute $C_2H_2Cl_4$ solutions; ^1H NMR spectra of PS-P4VP/PDP, PS-P4VP, and PDP in $CDCl_3$ and $C_2D_2Cl_4$; description and AFM images of nanostrand patterned films on other substrates. This material is available free of charge *via* the Internet at http://pubs.acs.org.

REFERENCES AND NOTES

1. Hamley, I. W. Nanotechnology with Soft Materials. *Angew. Chem., Int. Ed.* **2003**, *42*, 1692–1712.
2. Mendes, P. M.; Preece, J. A. Precision Chemical Engineering: Integrating Nanolithography and Nanoassembly. *Curr. Opin. Colloid Interface Sci.* **2004**, *9*, 236–248.
3. Hamley, I. W. Nanostructure Fabrication Using Block Copolymers. *Nanotechnology* **2003**, *14*, R39–R54.
4. Park, C.; Yoon, J.; Thomas, E. L. Enabling Nanotechnology with Self Assembled Block Copolymer Patterns. *Polymer* **2003**, *44*, 6725–6760.
5. Lazzari, M.; López-Quintela, M. A. Block Copolymers as a Tool for Nanomaterial Fabrication. *Adv. Mater.* **2003**, *15*, 1583–1594.
6. Li, M.; Coenjarts, C. A.; Ober, C. K. Patternable Block Copolymers. *Adv. Polym. Sci.* **2005**, *190*, 183–226.
7. Zhu, J.; Eisenberg, A.; Lennox, R. B. Interfacial Behavior of Block Polyelectrolytes. 1. Evidence for Novel Surface Micelle Formation. *J. Am. Chem. Soc.* **1991**, *113*, 5583–5588.
8. Zhu, J.; Lennox, R. B.; Eisenberg, A. Interfacial Behavior of Block Polyelectrolytes. 4. Polymorphism of (Quasi) Two-Dimensional Micelles. *J. Phys. Chem.* **1992**, *96*, 4727–4730.
9. Zhu, J.; Eisenberg, A.; Lennox, R. B. Interfacial Behavior of Block Polyelectrolytes. 5. Effect of Varying Block Lengths on the Properties of Surface Micelles. *Macromolecules* **1992**, *25*, 6547–6555.
10. Li, S.; Hanley, S.; Khan, I.; Varshney, S. K.; Eisenberg, A.; Lennox, R. B. Surface Micelle Formation at the Air/Water Interface from Nonionic Diblock Copolymers. *Langmuir* **1993**, *9*, 2243–2246.
11. Li, S.; Clarke, C. J.; Lennox, R. B.; Eisenberg, A. Two-Dimensional Self Assembly of Polystyrene-*b*-Poly(butylmethacrylate) Diblock Copolymers. *Colloids Surf. A* **1998**, *133*, 191–203.
12. Cox, J. K.; Yu, K.; Constantine, B.; Eisenberg, A.; Lennox, R. B. Polystyrene-Poly(ethylene oxide) Diblock Copolymers Form Well-Defined Surface Aggregates at the Air/Water Interface. *Langmuir* **1999**, *15*, 7714–7718.
13. Baker, S. M.; Leach, K. A.; Devereaux, C. E.; Gragson, D. E. Controlled Patterning of Diblock Copolymers by Monolayer Langmuir−Blodgett Deposition. *Macromolecules* **2000**, *33*, 5432–5436.
14. Seo, Y.; Im, J.-H.; Lee, J.-S.; Kim, J.-H. Aggregation Behaviors of a Polystyrene-*b*-Poly(methyl methacrylate) Diblock Copolymer at the Air/Water Interface. *Macromolecules* **2001**, *34*, 4842–4851.
15. Devereaux, C. A.; Baker, S. M. Surface Features in Langmuir-Blodgett Monolayers of Predominantly Hydrophobic Poly(styrene)−Poly(ethylene oxide) Diblock Copolymer. *Macromolecules* **2002**, *35*, 1921–1927.
16. Cheyne, R. B.; Moffitt, M. G. Novel Two-Dimensional "Ring and Chain" Morphologies in Langmuir−Blodgett Monolayers of PS-b-PEO Block Copolymers: Effect of Spreading Solution Concentration on Self-Assembly at the Air−Water Interface. *Langmuir* **2005**, *21*, 5453–5460.
17. Cheyne, R. B.; Moffitt, M. G. Self-Assembly of Polystyrene-block-Poly(ethylene oxide) Copolymers at the Air−Water Interface: Is Dewetting the Genesis of Surface Aggregate Formation. *Langmuir* **2006**, *22*, 8387–8396.
18. Kumaki, J.; Hashimoto, T. Two-Dimensional Microphase Separation of a Block Copolymer in a Langmuir−Blodgett Film. *J. Am. Chem. Soc.* **1998**, *120*, 423–424.
19. Park, J. Y.; Liu, M.; Mays, J.; Dadmun, M.; Advincula, R. Nano-Donuts from pH-Dependent Block Restructuring in Amphiphilic ABA Triblock Copolymers Vesicles at the Air/Water Interface. *Soft Matter* **2009**, *5*, 747–749.
20. Lopes, W. A. Nonequilibrium Self-Assembly of Metals on Diblock Copolymer Templates. *Phys. Rev. E* **2002**, *65*, 031606 (1−14).
21. van Zoelen, W.; ten Brinke, G. Thin Films of Complexed Block Copolymers. *Soft Matter.* **2009**, *5*, 1568–1582.
22. Nandan, B.; Gowd, E. B.; Bigall, N. C.; Eychmüller, A.; Formanek, P.; Simon, P.; Stamm, M. Arrays of Inorganic Nanodots and Nanowires Using Nanotemplates Based on Switchable Block Copolymer Supramolecular Assemblies. *Adv. Funct. Mater.* **2009**, *19*, 2805–2811.
23. Greiner, A.; Wendorff, G. H. Electrospinning: A Fascinating Method for the Preparation of Ultrathin Fibers. *Angew. Chem., Int. Ed.* **2007**, *46*, 5670–5703.
24. Lu, Q.; Bazuin, C. G. Solvent-Assisted Formation of Nanostrand Networks from Supramolecular Diblock Copolymer/Surfactant Complexes at the Air/Water Interface. *Nano Lett.* **2005**, *5*, 1309–1314.
25. Seo, Y.-S.; Kim, K. S.; Galambos, A.; Lammertink, R. G. H.; Vancso, G. J.; Sokolov, J.; Rafailovich, M. Nanowire and Mesh Conformations of Diblock Copolymer Blends at the Air/Water Interface. *Nano Lett.* **2004**, *4*, 483–486.
26. Kim, Y.; Pyun, J.; Fréchet, J. M. J.; Hawker, C. J.; Frank, C. W.

The Dramatic Effect of Architecture on the Self-Assembly of Block Copolymers at Interfaces. *Langmuir* **2005**, *21*, 10444–10458.
27. Chung, B.; Park, S.; Chang, T. HPLC Fractionation and Surface Micellization Behavior of Polystyrene-*b*-Poly(methyl methacrylate). *Macromolecules* **2005**, *38*, 6122–6127.
28. Price, E. W.; Guo, Y.; Wang, C.-W.; Moffitt, M. G. Block Copolymer Strands with Internal Microphase Separation Structure *via* Self-Assembly at the Air−Water Interface. *Langmuir* **2009**, *25*, 6398–6406.
29. Kadota, S.; Aoki, K.; Nagano, S.; Seki, T. Morphological Conversions of Nanostructures in Monolayers of an ABA Triblock Copolymer Having Azobenzene Moiety. *Colloid Surf. A* **2006**, *284*−*285*, 535–541.
30. Deschênes, L.; Bousmina, M.; Ritcey, A. M. Micellization of PEO/PS Block Copolymers at the Air/Water Interface: A Simple Model for Predicting the Size and Aggregation Number of Circular Surface Micelles. *Langmuir* **2008**, *24*, 3699–3708.
31. Xu, H.; Erhardt, R.; Abetz, V.; Müller, A. H. E.; Goedel, W. A. Janus Micelles at the Air/Water Interface. *Langmuir* **2001**, *17*, 6787–6793.
32. Peleshanko, S.; Jeong, J.; Gunawidjaja, R.; Tsukruk, V. V. Amphiphilic Heteroarm PEO-b-PS_m Star Polymers at the Air−Water Interface: Aggregation and Surface Morphology. *Macromolecules* **2004**, *37*, 6511–6522.
33. Matmour, R.; Francis, R.; Duran, R. S.; Gnanou, Y. Interfacial Behavior of Anionically Synthesized Amphiphilic Star Block Copolymers Based on Polybutadiene and Poly(ethylene oxide) at the Air/Water Interface. *Macromolecules* **2005**, *38*, 7754–7767.
34. Ruokolainen, J.; Saariaho, M.; Ikkala, O.; ten Brinke, G.; Thomas, E. L.; Torkkeli, M.; Serimaa, R. Supramolecular Routes to Hierarchical Structures: Comb−Coil Diblock Copolymers Organized with Two Length Scales. *Macromolecules* **1999**, *32*, 1152–1158.
35. Fasolka, M. J.; Mayes, A. M. Block Copolymer Thin Films: Physics and Applications. *Annu. Rev. Mater. Res.* **2001**, *31*, 323–355.
36. Hamley, I. W. Ordering in Thin Films of Block Copolymers: Fundamentals to Potential Applications. *Prog. Polym. Sci.* **2009**, *34*, 1161–1210.
37. Tokarev, I.; Krenek, R.; Burkov, Y; Schmeisser, D.; Sidorenko, A.; Minko, S.; Stamm, M. Microphase Separation in Thin Films of Poly(styrene-block-4-vinylpyridine) Copolymer-2-(4′-hydroxybenzeneazo)benzoic Acid Assembly. *Macromolecules* **2005**, *38*, 507–516.
38. Laforgue, A.; Gaspard, D.; Bazuin, C. G.; Prud'homme, R. E. Controlling Diblock Copolymer Nanopatterning and Nanoporosity on Surfaces Using Small Molecules. *Am. Chem. Soc. Polym. Prepr.* **2007**, *48* (1), 670–671.
39. van Zoelen, W.; Asumaa, T.; Ruokolainen, J.; Ikkala, O.; ten Brinke, G. Phase Behavior of Solvent Vapor Annealed Thin Films of PS-*b*-P4VP(PDP) Supramolecules. *Macromolecules* **2008**, *41*, 3199–3208.
40. van Zoelen, W.; Polushkin, E.; ten Brinke, G. Hierarchical Terrace Formation in PS-*b*-P4VP(PDP) Supramolecular Thin Films. *Macromolecules* **2008**, *41*, 8807–8814.
41. Tung, S.-H.; Kalarickal, N. C.; Mays, J. W.; Xu, T. Hierarchical Assemblies of Block-Copolymer-Based Supramolecules in Thin Films. *Macromolecules* **2008**, *41*, 6453–6462.
42. Meszaros, M.; Eisenberg, A.; Lennox, R. B. Block Copolymer Self-Assembly in Two Dimensions: Nanoscale Emulsions and Foams. *Faraday Discuss.* **1994**, *98*, 283–294.
43. Harirchian-Saei, S.; Wang, M. C. P.; Gates, B. D.; Moffitt, M. G. Patterning Block Copolymer Aggregates *via* Langmuir−Blodgett Transfer to Microcontact-Printed Substrates. *Langmuir* **2010**, *26*, 5998–6008.
44. Li, Z.; Zhao, W.; Quinn, J.; Rafailovich, M. H.; Sokolov, J.; Lennox, R. B.; Eisenberg, A.; Wu, X. Z.; Kim, M. W.; Sinha, S. K.; *et al*. X-ray Reflectivity of Diblock Copolymer Monolayers at the Air/Water Interface. *Langmuir* **1995**, *11*, 4785–4792.
45. Shin, K.; Rafailovich, M. H.; Sokolov, J.; Chang, D. M.; Cox, J. K.; Lennox, R. B.; Eisenberg, A.; Gibaud, A.; Huang, J.; Hsu, S. L.; *et al*. Observation of Surface Ordering of Alkyl Side Chains in Polystyrene/Polyelectrolytes Diblock Copolymer Langmuir Films. *Langmuir* **2001**, *17*, 4955–4961.
46. Nagano, S.; Matsushita, Y.; Ohnuma, Y.; Shinma, S.; Seki, T. Formation of a Highly Ordered Dot Array of Surface Micelles of a Block Copolymer *via* Liquid-Crystal-Hybridized Self-Assembly. *Langmuir* **2006**, *22*, 5233–5236.
47. Hosoi, A. E.; Kogan, D.; Devereaux, C. E.; Bernoff, A. J.; Baker, S. M. Two-Dimensional Self-Assembly in Diblock Copolymers. *Phys. Rev. Lett.* **2005**, *95*, 037801(1−4).
48. Chung, B.; Choi, M.; Ree, M.; Jung, J. C.; Zin, W. C.; Chang, T. Subphase pH Effect on Surface Micelle of Polystyrene-*b*-Poly(2-vinylpyridine) Diblock Copolymers at the Air−Water Interface. *Macromolecules* **2006**, *39*, 684–689.
49. Fahmi, A. W.; Braun, H.-G.; Stamm, M. Fabrication of Metallized Nanowires from Self-Assembled Diblock Copolymer Templates. *Adv. Mater.* **2003**, *15*, 1201–1204.